INTERNATIONAL JOURNAL OF
COASTAL & OFFSHORE ENGINEERING
IJCOE No. 4 / Autumn 2016 (1-10)

Numerical Simulation of Vortex Induced Vibration of Three Cylinders in Regular Triangle Arrangement at High Reynolds Number

Hassan Sayyaadi [1], Abolfazl Motekallem[2]

[1]*Professor, Center of Excellence in Hydrodynamics and Dynamics of Marine Vehicles, Sharif University of Technology/ Scholl of Mechanical Engineering; Sayyaadi@sharif.edu*
[2] *M.Sc. student, Sharif University of Technology/ School of Mechanical Engineering; Motekallem_Abolfazl@mech.sharif.edu*

ARTICLE INFO

Article History:
Received: 11 Sep. 2016
Accepted: 15 Dec. 2016

Keywords:
Fluids Structure Interaction (FSI)
Workbench System Coupling
Vortex Induced Vibration,
Numerical Method
Karman Vortex Shedding

ABSTRACT

This paper presents a three dimensional simulation of the vortex induced vibrations of three elastic cylinders in regular triangle arrangement at high Reynolds number. The motion of every single cylinder, which is free to oscillate in two degrees of freedom in a uniform flow and has the same mass and natural frequency in both X and Y directions, is modeled by a mass spring damping system. The displacement and lift forces for each cylinder are analyzed with five spacing ratios L/D changing from 2.5 to 6.5. The results indicate that the downstream cylinders are usually undergone serious fluctuating lift forces. It is found that the simultaneous resonance in the X and Y directions may occur for the downstream cylinders.
The stream wise oscillation of downstream cylinders could be as large as 0.54D, and the maximum transverse amplitude of three cylinders can reach to 2.30D. It is indicated that the cross flow oscillation amplitude of three cylinders significantly increased compared with the flow induced vibration of a single elastic cylinder and the stream wise oscillation of downstream cylinders is unneglectable for vortex induced vibration of multi cylinder system.

1. Introduction

The viability and accuracy of large eddy simulation (LES) with wall modeling for high Reynolds number complex turbulent flows is investigated by Pietro Catalano (2003), considering the flow around a circular cylinder in the super critical regime (5×10^5 and 10^6) [1]. Guilmineau (2004) present some numerical results from a study of the dynamics and fluid forcing on an elastically mounted rigid cylinder with low mass damping, constrained to oscillate transversely to a free stream [2]. Z. Huang (2006) had performed a systematic study of flow around one cylinder, two side by side cylinders, one row of cylinders and two rows of cylinders [3]. Experimental measurements and large eddy simulation (LES) technique were used by K. Lam to study the turbulent flow characteristics in a staggered tube bundle arrangement in 2010 at a subcritical Reynolds number of Re=7500 [4]. K. Lam presents the results of an investigation on the effects of wavy cylindrical tubes in a staggered heat exchanger tube bundle. The aim of this investigation is to compare the flow characteristics of a new configuration of cylindrical tubes with that of a similar arrangement which comprises purely circular cylinders. For the flow induced vibration problem some numerical work also carried out. A numerical study has been carried out by S. Mittal to study the flow induced vibrations of a pair of cylinders in tandem and staggered arrangements at Re=100 [5]. Detailed numerical results for the flow patterns for different arrangements of the cylinders, at a Reynolds number, Re=800, are presented. Several qualitatively distinct wake regimes were observed experimentally as well as numerically by F.L. Ponta (2006) [6]. In year 1996, C.H.K. Williamson had studied the three dimensional vortex behavior of flow past a bluff body [7]. Results predict that for a low Reynolds number flow ($Re < 260$) in wake region of the bluff body the flow remains two dimensional behavior. For $Re > 260$ the vortex generated due to flow past a bluff body having a three dimensional nature of flow.
In summary, thus, many experimental as well as numerical work at higher Reynolds no is done in FIV area. Some of them have calculated the FIV and suggested the techniques to damp the vibration, where

as some work are done experimentally by changing orientation of tube bundle in triangular array. Literatures also suggest the appropriate condition to setup the model of FIV. In spite of all these studies, the investigations of flow induced vibrations as a fully coupled problem are still incomplete. In addition, little theoretical work has been done for the simulation and control of flow induced vibrations

1. Numerical Method

The simulation associated with VIV includes the unsteady fluid flow and the motion of the cylinder. The interaction between fluid and cylinder is significant to the process.

2.1 The governing equations

The governing equations of fluid are the unsteady and viscous Navier Stokes equations written in terms of conservative variables. The continuity, momentum and energy equations are as follows:

$$\frac{\partial \rho}{\partial t} + \frac{\partial (\rho u_k)}{\partial x_k} = 0 \tag{1}$$

$$\frac{\partial (\rho u_i)}{\partial} + \frac{\partial (\rho u_i u_k + p\delta_{ik} - \tau_{ik})}{\partial x_k} = 0 \tag{2}$$

$$\frac{\partial E}{\partial t} + \frac{\partial [u_k (E + p) - \tau_{ik} u_i + Q_k]}{\partial x_k} = 0 \tag{3}$$

where the velocity components by u_k and the relationship for the total energy E is given by

$$E = \frac{p}{\gamma - 1} + \frac{1}{2}\rho u_k u_k \tag{4}$$

where γ is the specific heat capacity ratio, p is the pressure. The heat flux and stress tensor are given by

$$Q_k = -\frac{\gamma}{(\gamma - 1) RePr} \frac{\partial T}{\partial x_k} \tag{5}$$

$$\tau_{ik} = \frac{1}{Re}\left(\frac{\partial u_i}{\partial x_k} + \frac{\partial u_i}{\partial x_k}\right) - \frac{2}{3}\frac{1}{Re}\delta_{ik}\frac{\partial u_j}{\partial x_j} \tag{6}$$

where $\Pr = 0.72$ and Re are Prandtl and Reynolds numbers. The 2nd order finite difference is used as the spatial discretization scheme. The third order Runge Kutta scheme is applied for the temporal discretization. The immersed boundary method uses a regular Eulerian computational grid for the fluid mechanics together with a Lagrangian representation of the immersed boundary. Boundary movement to the orthogonal mesh can be simply done by changing the coordinates of boundary points without any adjustment to the basic grid, so the immersed boundary methods do not cost additional time for regridding. The boundary condition of velocity on the body surface is

$$u_f = u_b \tag{7}$$

where u_f is the velocity of fluid at a point on the surface, $u_b$is the velocity of this point on the body. An adiabatic boundary condition is used for temperature in the present work. The critical problem for the computation is implementing the boundary conditions for a body nonconformal grid. Instead of a curvilinear body nonconformal grid used by Ghias et al [8], an orthogonal body nonconformal grid is used as shown in Fig. 1. In the present work, some modifications are made for implementing the boundary conditions. In Fig. 1, the p_1 is a typical point whose parameters cannot be calculated by solving Eqs. (1)-(3). The parameters at this point have to be interpolated from the solid surface p_s and point p_2. The line $p_s p_2$ is across point p_1 and perpendicular to the solid surface. Point p_1 is on the solid surface, at which the velocity $(u_{s-x}.u_{s-y})$ is known. The velocity at point p_2 is $(u_{2-x}.u_{2-y})$,which can be interpolated from local grid $(i_0.j_0).(i_0+1.j_0).(i_0+1.j_0+1)$ and $(i_0+1.j_0+1)$. The u_{2-x}can be expressed as

$$u_{2-x} = \sum_{i=i_0}^{i_0+1}\sum_{j=j_0}^{j_0+1} \delta\left(\frac{h_x}{h}\right)\delta\left(\frac{h_y}{h}\right)(u_x)_{ij} \tag{8}$$

where the delta function is defined as

$$\delta(x) = \begin{cases} 1 - |x| & |x| < 1 \\ 0 & |x| \geq 1 \end{cases} \tag{9}$$

Here h_x denotes the element size near the solid surface. h_x and h_y are the distances between point p_2 and adjacent grid in the X and Y direction, respectively. Then, the u_{1-x} at u_1 can be calculated by

$$u_{1-x} = \frac{l_1}{l}u_{2-x} + \frac{l_2}{l}u_{s-x} \tag{10}$$

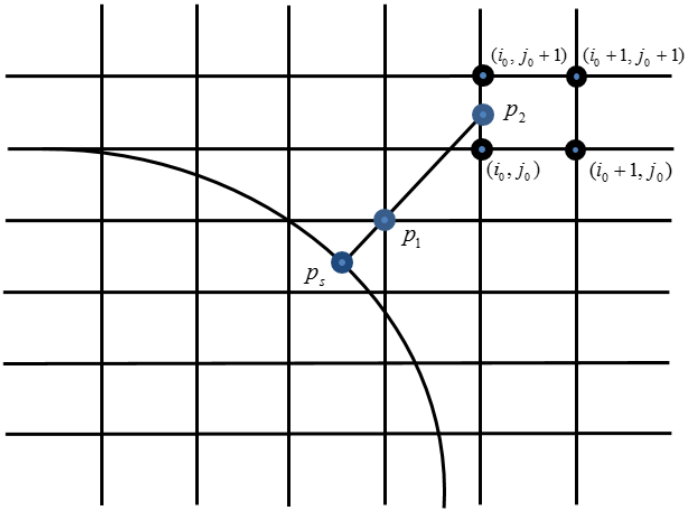

Fig. 1. Schematic showing an immersed boundary on an orthogonal body nonconformal grid.

where l_1 is the distance between points p_1 and p_s, and l_2 is the distance between points p_1 and p_2. l is $l_1 + l_2 + l_3$ set to $1 \cdot 5h$, which ensures that the interpolation of parameters at point p_2 is independent of parameters at point p_1. Temperature at p_1 is determined by assuming adiabatic condition at Point p_s and the density is determined by applying the equation of state at the wall.

In this simulation, drag and lift force coefficients are used to quantify the hydrodynamic characteristics. The definitions are also given here:

$$C_x = \frac{F_x}{\frac{1}{2}\rho U^2 DL} \tag{11}$$

$$C_y = \frac{F_y}{\frac{1}{2}\rho U^2 DL} \tag{12}$$

Here F_x and F_y are the fluid forces exerted on the bodies, respectively, in streamwise and transverse directions and are calculated by performing an integration along the wall, involving both pressure and viscous effects:

$$F_x = -\int_S (pn + \mu n \times \omega) n_x da \tag{13}$$

$$F_y = -\int_S (pn + \mu n \times \omega) n_y da \tag{14}$$

where $\omega = \nabla u$, whose value is calculated from the velocities at points p_s and p_2 in Fig. 1. The pressure on the surface is extrapolated from the interior of the flow onto the boundary. **n** denotes the outward unit normal to the cylinder surface. n_x and n_y are the Cartesian components of $\boldsymbol{n} \cdot S$ represents the cylinder surface. In order to analyze the aerodynamic behavior of VIV, we define the instantaneous potential added-mass and vortex force coefficients as

$$C_{Potential}(t) = 2\pi^3 \frac{[y(t)/D]}{(U^*/f^*)^2} \tag{15}$$

$$C_{Vortex}(t) = C_y(t) - C_{Potential}(t) \tag{16}$$

which are same as the definitions used by Govardhan and Williamson [9], $C_{Potenial}(t)$ is always in phase with the cylinder motion $y(t)$. Frequency ratio $f^* = f/f_N$; reduced velocity $U^* = U/f_N D$; and y is the displacement in transverse direction.

2.2. The equations for a rigid cylinder

The motion of the elastically mounted rigid cylinder is restricted in the transverse direction (Y axis in the present simulation), and is governed by

Vibration equations,

$$m\ddot{x} + c\dot{x} + kx = F \tag{17}$$

Force in X direction,

$$m\ddot{x} + c\dot{x} + kx = F_x \tag{18}$$

Force in Y direction,

$$m\ddot{x} + c\dot{x} + kx = F_y \tag{19}$$

Where, the forces F_x and F_y are the total drag and lift forces acting on the cylinder and ,c and k are the tube

mass per unit length, structural damping coefficient and spring constant respectively.

Drag and Lift coefficient,

$$C_D = \frac{F_D}{\frac{1}{2}\rho U_\infty^2 D} \tag{20}$$

$$C_L = \frac{F_L}{\frac{1}{2}\rho U_\infty^2 D} \tag{21}$$

Where, F_x and F_y are the total drag and lift forces exerted by the fluid acting on cylinder per unit cylinder length. Therefore $C_D = C_{DP} + C_{DF}$where C_{DP} and C_{DF} are pressure and friction drag coefficients respectively. The frequency of vortex shedding (f) in wake region is given by Strouhal number (St) and it is defined as

$$St = \frac{fD}{U_\infty} \tag{22}$$

Vortex shedding from a smooth, circular cylinder in a steady flow is a function of Reynolds number. The Reynolds number is based on free stream velocity *U* and cylinder diameter *D,*

$$Re = \frac{\rho U_\infty D}{\mu} \tag{23}$$

The cylinder has been modeled as a two degree of freedom system with independent responses in X the drag direction, and Y the lift direction. The initial conditions of the cylinder are zero displacement and velocity. As discussed in the introduction, the response is assumed to be two dimensional with symmetry along the cylinder axis. The following properties are applied:

k - Stiffness is 25.5742 N/m
m - Mass per unit length is 7.804kg/m

2. FSI Solution of ANSYS

The VIV behavior of a circular cylinder is simulated by a transient coupled FSI numerical model using the combination of CFX and ANSYS transient structure platforms. The well designed FSI solution scheme provides tight integrations between hydrodynamics and structural physics, offering a flexible, advanced structure fluid analysis tool. The geometry module provides a geometric model for the transient structure solver and the ANSYS CFX solver. Coupled simulations begin with the execution of the ANSYS transient structure and ANSYS CFX solvers. The system coupling solver acts as a coupling master process to which the transient structure solver and ANSYS CFX solvers connect. Once that connection is established, the solvers advance through a sequence of predefined synchronization points (SP). At each of these SPs, the ANSYS CFX solver transfers the fluid dynamic loads data to the transient structure solver based on the system coupling solver; in turn, the transient structure solver transfers the structure response data to the ANSYS CFX solver also based on the system coupling solver. Finally, the mesh is updated with the diffusion based smoothing method based on the response of the cylinder. The coupled simulation proceeds in time during the outer loop. Staggered iterations are repeated until a maximum number of stagger iterations is reached or until the data transferred between solvers and all field equations have converged. The adoption of implicit coupling iteration ensures that fluid and structure solution fields are consistent with each other at the end of each multi field step, leading to improved numerical solution stability.

3. Problem Definition

Consider unsteady, three dimensional, viscous, incompressible flow past triangular array of circular cylinder placed in a uniform stream, as shown schematically in Fig. 2. The flow is bounded by the plane at upper and lower side boundaries.

These are treated as symmetry boundary condition, while vertical plane at left side and vertical plane right of the domain are considered as the flow inlet and outlet planes respectively. Free stream velocity is specified as 0.5 m/s at the inflow boundary. Three stationary cylinders are placed in triangular array, two downstream sides and one upstream side. The cylinder wall is considered as no slip boundary condition (Fig. 2). Consider upper downstream side cylinder as cylinder D.U. Riser, lower downstream side cylinder as cylinder D.D. Riser and upstream cylinder as cylinder U. Riser hereafter. All three stationary circular cylinders are of diameter D (D=0.1m). It is observed from Fig. 2 that upstream cylinders were placed at 10D and 30D distance away from the inlet and outlet boundaries, respectively. Five different (L/D = 2.5 to 6.5) considered in the present study.

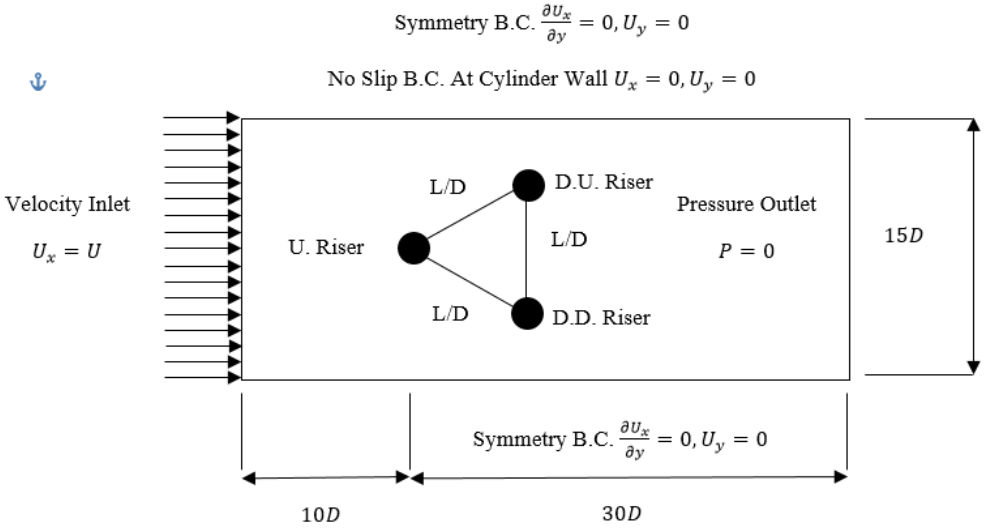

Fig. 2. Schematic of 2 DOF computational domains.

4. Mesh Validation

Mesh dependency study was carried out and it has been demonstrated that further increasing in mesh density makes little difference on the results for the Strouhal numbers simulated. Fig. 3 shows the computational domain as well as the generated grid (for one of the test cases). The size of the domain used in the numerical investigation was 40D×15D. In order to set up a grid independent solution, numerical simulations have been conducted for different meshes and the optimum mesh consisted of 272840 quadrilateral elements, with a finer mesh employed near the boundary layer to capture the flow behavior, since the boundary layer flow patterns are significant in this investigation. The number and type of mesh elements have been selected in an iterative solution with a minimal time step to obtain an accurate solution.

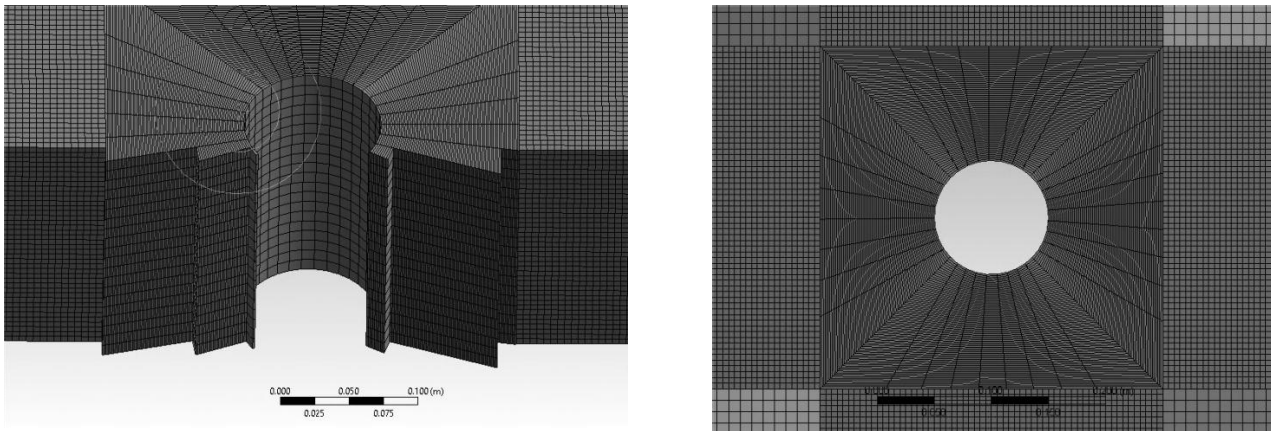

(a) (b)

Fig. 3. (a). Three dimensional grids near the cylinders, (b). Horizontal section of grids near the cylinders.

The same geometry and mesh elements, as well as initial and boundary conditions, were used for all numerical simulations. Based on the mesh size and the free stream velocity, the selected time step was kept constant in all simulations, $\Delta t = 0 \cdot 005 s$. Based on this time step the maximum number of iterations per each time step was 25. To reach solution convergence of the computational analyses the residual target of $10 - 5$was considered. In addition, the lift and drag coefficients on the cylinders were monitored during the computational process and sinusoidal behavior of these coefficients was taken into account to accompany the convergence criterion. Furthermore, a grid independent study was conducted with several mesh elements qualities for one of the test cases (L/D=2.5). Here, the mesh refinement sensitivity is summarized in Table 1. According to the findings, the refined mesh was chosen for the rest of the simulations and LES turbulence models were used to investigate the turbulent flow behavior around the three cylinders.

Table 1: Mesh Dependence Study at $Re = 4 \cdot 97 \times 10^5$ and $U^* = 5 \cdot 5$ for different meshes.

Mesh Case	Number of Elements	Lift Frequency	Drag Frequency	f_x/f_y	Strouhal Number
1	122700	0.75	1.56	2.08	0.15
2	272840	0.85	1.71	2.01	0.17
3	491250	0.85	1.76	2.07	0.17

5. Model Validation

Firstly, the flow around a rigid cylinder at $Re = 1 \cdot 1 \times 10e5$ is carried out in order to ensure the reliability of numerical calculation. In Fig. 4, high Reynolds number ($Re > 4 \times 10e5$) VIV data obtained through UTM experiments are presented along with results calculated through CFD simulations. The results in Fig. 4 are showing the ability of ANSYS CFX for detecting the oscillating behavior and nearly the same vertical displacement for the cylindrical riser as that for the experimental results at UR = 6.0. However, there is a noticeable irregular phase shift between the numerical and the experimental. Where the uniform flow condition was imposed exactly at the inlet boundary condition at all CFD simulations in this study, while in the experimental tests in UTM towing tank this uniform flow condition cannot be attained exactly. In addition, this miss matching between the experimental and the numerical results can also be attributed to the inability of the turbulence models even with the use of LES for predicting precisely the complex flow pattern of VIV for such cases [10]. Results shows maximum error between the numerical simulation and the experimental in lift coefficient is %16 at UR = 5.0. It is shown that the grid resolution, time step and numerical solving format chosen in present paper are proper for numerical simulation of the flow around the cylinder.

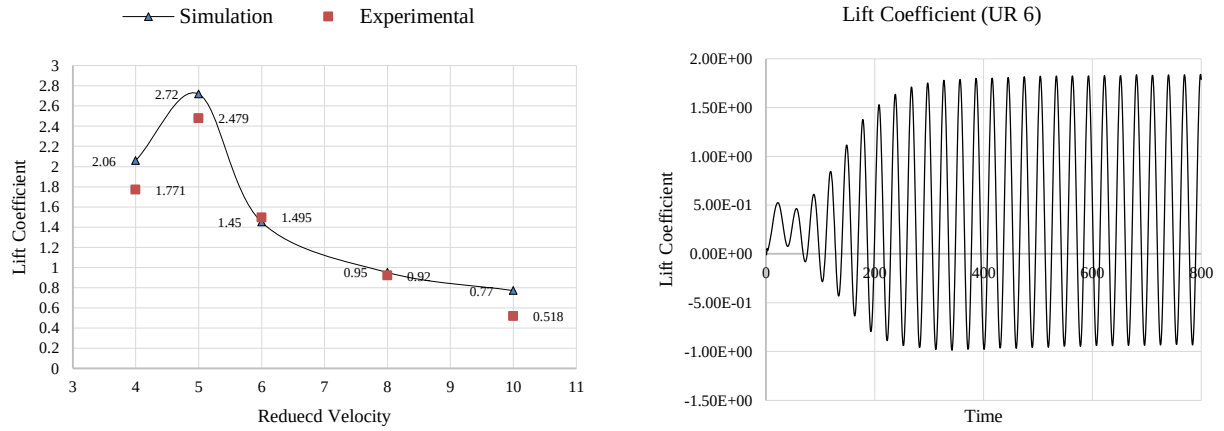

Fig. 4. Amplitude response of an elastically mounted circular cylinder in fluid flow.

6. Result and Discussion

Fig. 5 shows the force coefficients vary as the spacing ratio for three cylinders in regular triangle arrangement, which include the mean value of lift coefficient C_l. Fig. 5 indicates that the mean lift coefficients of downstream cylinders D.U. Riser and D.D. Riser are equal to each other in magnitude with opposite direction. It is seen that C_l D.U. Riser is positive and C_l D.D. Riser is negative, and the C_l U. Riser has positive negative value for L/D=2.5~5.5. All lift coefficient mean values gradually trend to zero as L/D increasing, and it indicates that the flow interference effects between upper and lower rows cylinders is gradually weakened as spacing increasing.

The ratio of cross flow displacement mean values to diameter is shown in Fig. 6. The ratio of the inflow displacement mean values to diameter is shown in Fig. 7(a) and Fig. 7(b), respectively. In Fig. 6, the cross flow displacement mean Y of each cylinder express same trend with the lift coefficients as shown in Fig. 5. When the L/D changes from 2.5 to 3.5, the Y magnitude of each cylinder obviously increase. In the region of L/D=2.5~3.5, the cross flow displacement amplitude of U. Riser, D.U. Riser and D.D. Riser reach their maximum values with 0.47, 2.30 and 1.92 times of cylinder diameter, respectively.

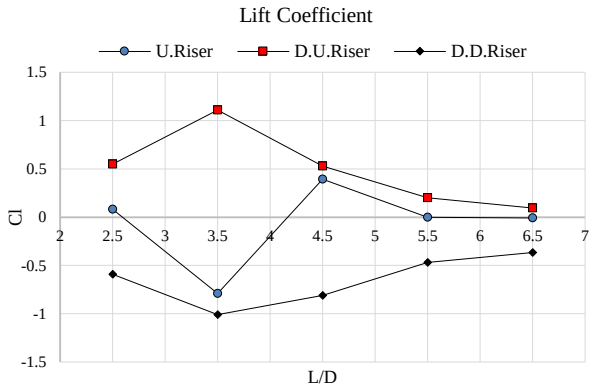

Fig. 5. Mean values of lift coefficients versus L/D.

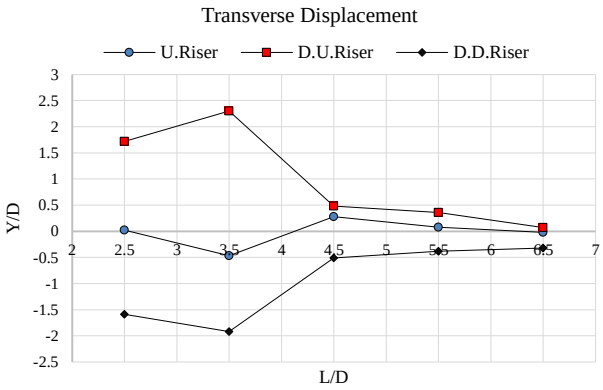

Fig. 6. Mean values of Y directions displacement versus L/D

In Fig. 7(a), it can be seen that the inflow displacement means $X_{D.U.\ Riser}$, $X_{D.D.\ Riser}$ of downstream cylinders have the same changing trend and increase in the all L/D range. The $X_{U.\ Riser}$ of upstream cylinder gradually increases from 0.31 to 0.64 as L/D increases and reaches the maximum value at L/D=6.5 that shown in Fig. 7(b).

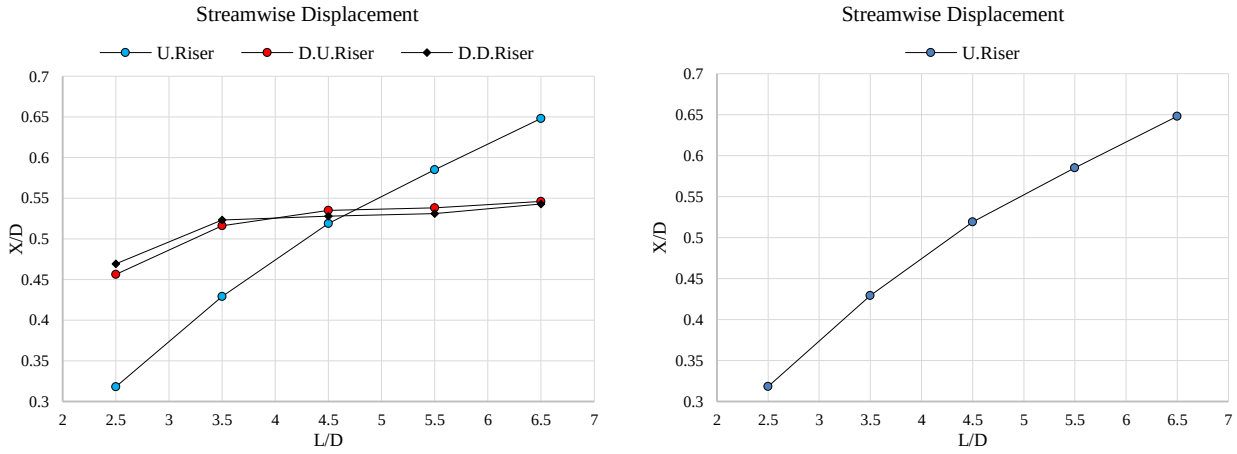

(a) (b)

Fig. 7. (a). Mean values of X directions displacement versus L/D, (b). Mean values of $X_{U.\ Riser}$ directions displacement versus L/D

Finally, contours of flow velocity of the model are shown in Fig. 8 to 11. The distance between the spacing ratio is considered L/D=3.5 that have maximum cross flow displacement. The velocity contours are shown when the oscillating cylinders are at their uppermost and lowermost positions. Fig. 8 shows the results for L/D=3.5 when all cylinders are at their minimum position in X direction and Fig. 9 shows the same contours for the maximum position in X direction. As it can be seen, the movement of downstream cylinders is more than upstream cylinder and also another thing that should be mention is the upstream cylinder never goes behind the reference point and all of its movements are in right hand of the reference point. In the other hand, the downstream cylinders, moves either in left or right hand of the reference point. The maximum amplitude for upstream cylinder in X direction is almost 0.64D and for downstream cylinders is slightly below 0.54D.

Fig. 10 shows the results for L/D=3.5 when the both cylinders are at their minimum positions in Y direction and Fig. 11 the same results when they are at their maximum positions in Y direction. For the upstream cylinder the maximum amplitude is about 0.47D and for downstream cylinders is almost 2.30 and 1.92 for D.U. Riser and D.D. Riser, respectively. It shows that downstream cylinders at L/D=3.5, have the same of movement and this is the exception because as can be seen in Fig.6, at all other spacing ratio, there are a different amplitude in Y direction for cylinders. Also the counter of velocity shows that the shear layers roll down after the downstream body and roll up after the upstream body.

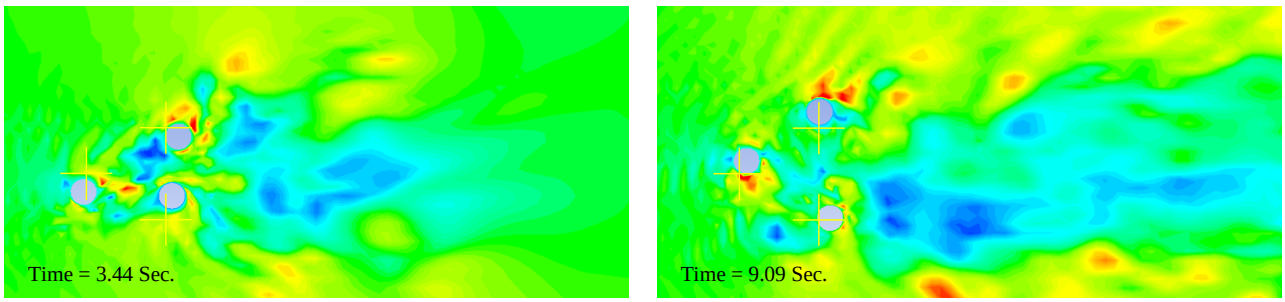

(a) (b)

Fig. 8. Velocity contours of three cylinders in triangle arrangement, L/D=3.5; Lowermost position of (a). Upstream cylinder in X direction, (b). Downstream cylinders in X direction

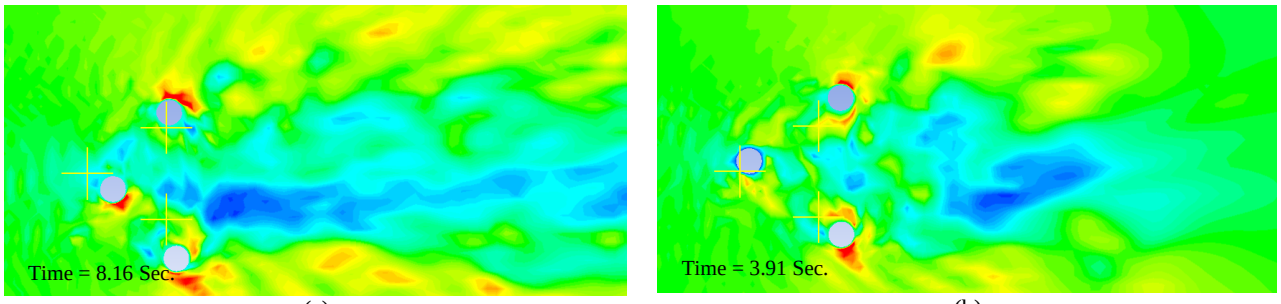

(a) (b)

Fig. 9. Velocity contours of three cylinders in triangle arrangement, L/D=3.5; Uppermost position of (a). Upstream cylinder in X direction, (b). Downstream cylinders in X direction

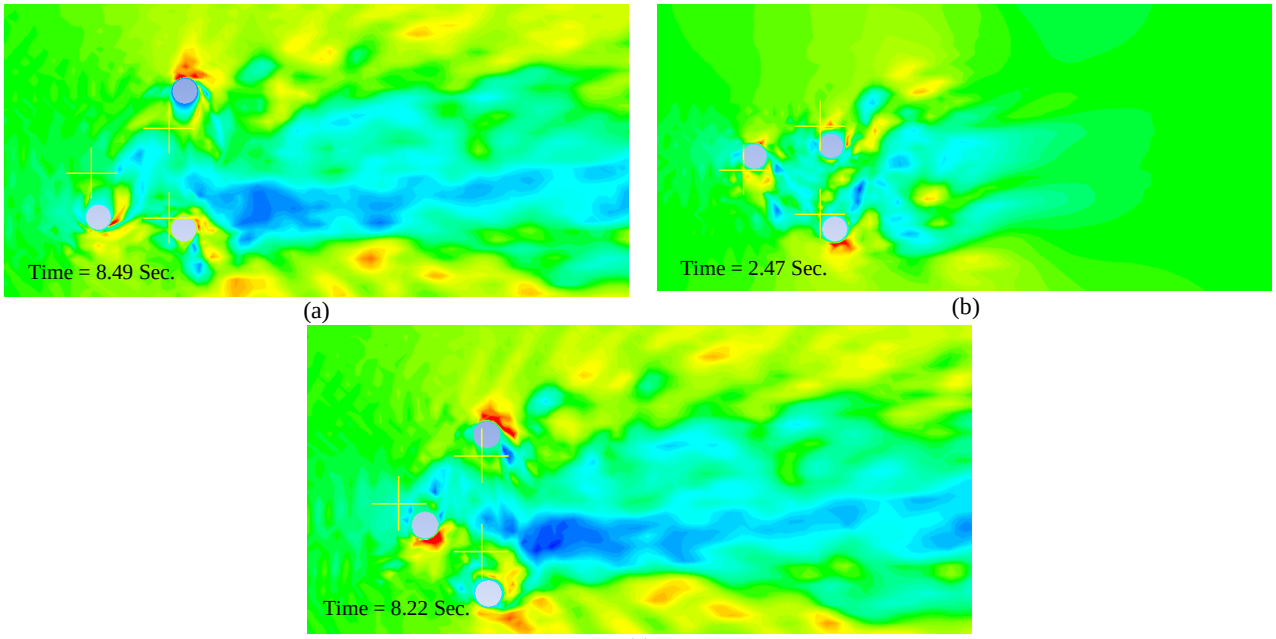

(a) (b)

(c)

Fig. 10. Velocity contours of three cylinders in triangle arrangement, L/D=3.5; Lowermost position of (a). Upstream cylinder in Y direction, (b). Downstream cylinder (D.U. Riser) in Y direction, (c). Downstream cylinder (D.D. Riser) in Y direction

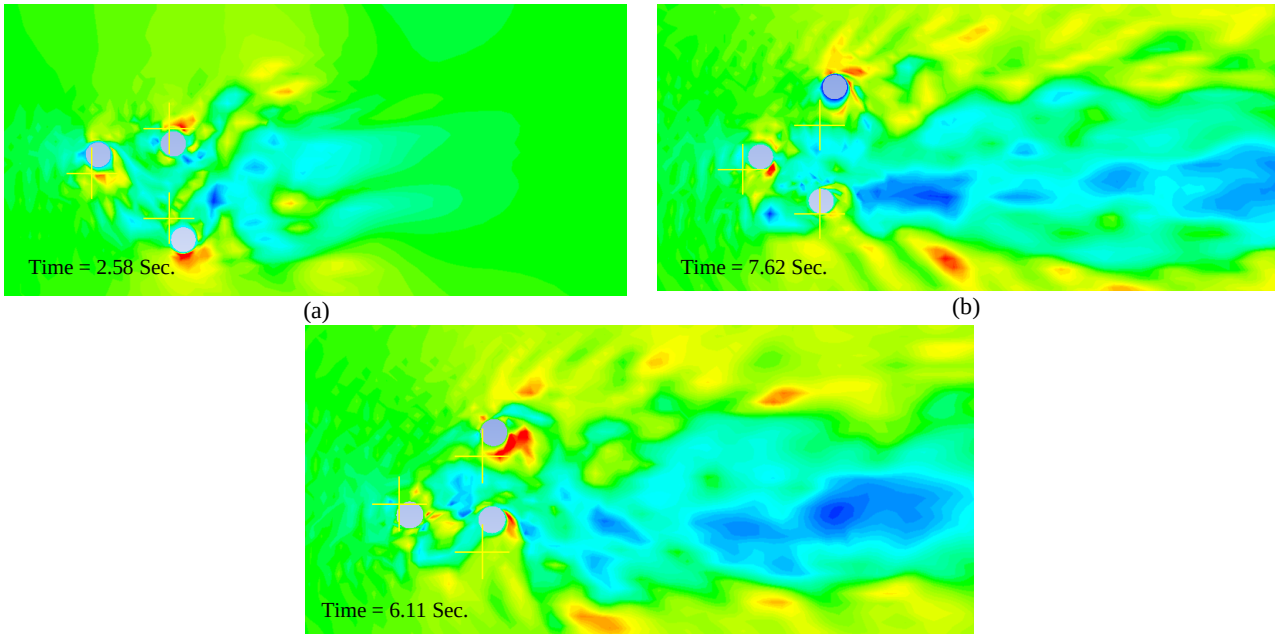

Fig. 11. Velocity contours of three cylinders in triangle arrangement, L/D=3.5; Uppermost position of (a). Upstream cylinder in Y direction, (b). Downstream cylinder (D.U. Riser) in Y direction, (c). Downstream cylinder (D.D. Riser) in Y direction

Conclusion

This paper presents a feasible research method for numerical simulation of vortex induced vibration of elastic multi cylinder oscillating system. The fluid domain simulation is completed by ANSYS CFX, the structure response is achieved using the LES turbulence method and the grid domain updating is accomplished through a dynamic mesh method. The mass ratio, reduced damping and frequency ratio are kept invariant and the emphasis analysis is carried out for influence of the spacing ratio variety to lift forces, vibrating responses and wake vortex modes of three cylinders in regular triangle configuration. The following conclusions are obtained from this study:

(1) As the spacing ratios increasing, the mean lift coefficient of each cylinder trends to zero. The fluctuating lift coefficients of downstream cylinders are larger than those of upstream cylinder for all range of spacing ratios.

(2) In all L/D range, the fluctuation of the transverse displacement (Y) is very close to each other, and the fluctuating stream wise displacement of downstream cylinders (X) is larger than that of upstream cylinder.

(3) The maximum transverse oscillation amplitude of three cylinders can be reached 2.30D which is much larger than that of the single cylinder undergoing VIV with the same parameters setting. On the other hand, the maximum stream wise fluctuating amplitude of the downstream cylinders reaches 0.54D. It is indicated that the transverse oscillation amplitude of downstream cylinders significantly increased and the stream wise oscillation of upstream cylinder is unneglectable for vortex induced vibration of multi cylinder system.

List of Symbols

Re	Reynolds Number
St	Strouhal Number
C_L	Lift Coefficient
C_D	Drag Coefficient
ρ	Density
μ	Fluid Viscosity
k	Stiffness
ζ	Structural damping
m	Mass per unit length
l	Length
D	Diameter
U_∞	Fluid Viscosity
F_l	Lift Force
F_D	Drag Force
f	Lift Coefficient Frequency
U^*	reduced velocity

References

[1] Catalano P., Wang M., Iaccarino G., Moin P.," Numerical Simulation of the flow around a circular cylinder at high Reynolds number". International Journal of Heat and Fluid Flow (2003) 24, 463-469.

[2] Guilmineau E., Queutey P.," Numerical simulation of vortex induced vibration of circular cylinder with low mass damping in a turbulent flow". Journal of Fluids and structures 19 (2004), 449-466.

[3] Huang Z., Olson J.A., Kerekes R.J., Green S.I.," Numerical simulation of the flow around rows of cylinders", Computers and Fluids 35 (2006), 485-491.
[4] Lam K., Lin Y.F., Zou L., Liu Y.," Experimental study and large eddy simulation of turbulent flow around tube bundles composed of wavy and circular cylinders". International Journal of Heat and Fluid 31 (2010)32-44.
[5] Mittal S., Kumar V.," Flow induced vibration of circular cylinder in tandem and staggered arrangement", Journal of Fluids and Structures 15 (2001), 717-736.
[6] Ponta F.L., Aref H.," Numerical experiments on vortex shedding from an oscillating cylinder", Journal of Fluids and Structures 22 (2006), 327-344.
[7] Williamson C.H.K.," Three dimensional vortex dynamics in bluff body wakes", Experimental Thermal and Fluid Science 12(1996), 150-168.
[8] Ghias, R., Mittal, R., Dong, H.," A sharp interface immersed boundary method for compressible viscous flows", Journal of Computational Physics 225(2006), 528–553.
[9] Govardhan, R., Williamson, C.H.K.," Modes of vortex formation and frequency response for a freely vibrating cylinder", Journal of Fluid Mechanics 420(2000), 85–130.
[10] F. Saltara, A. D. Agostini Nato, J. I. Z Lopez. 2011. 3D CFD Simulation of Vortex induced Vibration of Cylinder. International Journal of Offshore and Polar Engineering. 21(3): 192–197.